Published in final edited form as:

Mol Pharm. 2020 December 07; 17(12): 4629–4636. doi:10.1021/acs.molpharmaceut.0c00834.

Cisplatin Prodrug-Loaded Nanoparticles Based on Physalis Mottle Virus for Cancer Therapy

He Hu,

Department of NanoEngineering, University of California-San Diego, La Jolla, California 92093, United States

Nicole F. Steinmetz*

Department of NanoEngineering, Department of Bioengineering, Department of Radiology, Moores Cancer Center, and Center for Nano-ImmunoEngineering, University of California-San Diego, La Jolla, California 92093, United States

Abstract

Nanoparticle-based prodrugs offer an effective strategy to improve the safety and delivery of small-molecule therapeutics while reducing the risk of drug resistance. Here, we conjugated a maleimide-functionalized cisplatin prodrug containing Pt(IV) to the internal and/or external surface of virus-like particles (VLPs) derived from Physalis mottle virus (PhMV) to develop a pH-sensitive drug delivery system. The internally loaded and PEGylated VLPs (Pt-PhMVCy5.5-PEG) were taken up efficiently by cancer cells where they released platinum, presumably as a reduced, DNA-reactive Pt(II) complex, rapidly under acidic conditions *in vitro* (>80% in 30 h). The efficacy of the VLP-based drug delivery system was demonstrated against a panel of cancer cell lines, including cell lines resistant to platinum therapy. Furthermore, Pt-PhMVCy5.5-PEG successfully inhibited the growth of xenograft MDA-MB-231 breast tumors *in vivo* and significantly prolonged the survival of mice compared to free cisplatin and cisplatin-maleimide. Pt-PhMVCy5.5-PEG therefore appears promising as a prodrug to overcome the limitations of conventional platinum-based drugs for cancer therapy.

Graphical Abstract

***Corresponding Author**: nsteinmetz@ucsd.edu.

ASSOCIATED CONTENT

Supporting Information

The Supporting Information is available free of charge at https://pubs.acs.org/doi/10.1021/acs.molpharmaceut.0c00834.

Synthesis of platinum compounds; VLP characterization methods; kinetics of Pt release; IC_{50} profiles of four cancer cells treated with different VLPs; LCSM imaging and FACS analysis of PC-3 cells; and tumor growth curves of individual mice (PDF)

Complete contact information is available at: https://pubs.acs.org/10.1021/acs.molpharmaceut.0c00834

The authors declare no competing financial interest.

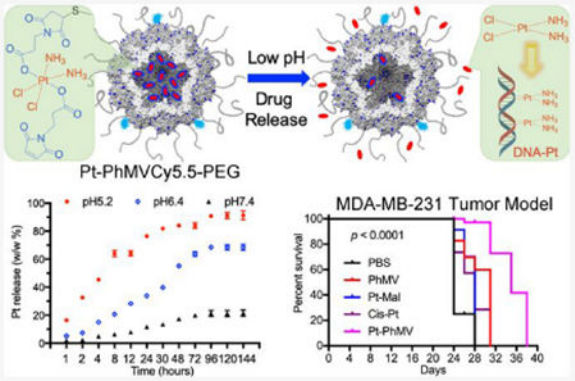

Keywords

cisplatin resistance; pH-responsive drug delivery; prodrug; nanomedicine; plant virus-like nanoparticles

INTRODUCTION

Cancer affects more than 90 million people and kills almost 9 million every year.[1] Chemotherapy is a primary treatment option, either as monotherapy or combined with radiotherapy surgery and other treatment options.[2] Among the wide variety of approved chemotherapy reagents, *cis*-diamminedichlorido-platinum(II) (cisplatin) is one of the most effective for the treatment of solid tumors, including breast cancer.[3] The proposed mechanism of action involves the formation of DNA adducts.[4] However, some tumor cells acquire cisplatin resistance by limiting drug uptake, enhancing drug deactivation or efflux, or repairing platinated DNA.[5] Furthermore, cisplatin causes off-target effects by damaging healthy cells, reflecting its undesirable pharmacokinetic behavior and biodistribution.[2] It is therefore of interest to develop new drug formulations that promote the efficacy of cisplatin while reducing the likelihood of resistance emerging in the target cell population.

The drawbacks of cisplatin can be addressed using a nanoparticle-based prodrug delivery system (NPDDS) in which small-molecule therapeutics are encapsulated by or conjugated to nanoparticles in order to improve their pharmacokinetic properties via enhanced permeability and retention (EPR) or active targeting, thus increasing their efficacy.[6] Several NPDDS formats have been developed for the delivery of platinum-based drugs, including polymers,[7] liposomes,[8] single-walled carbon nanotubes,[9] gold nanoparticles,[9] metal—organic frameworks,[10] and mesoporous silica nanoparticles.[11] Some of these formulations have been tested in clinical trials;[12,13] this also includes the albumin-binding cisplatin prodrug BTP-114 (https://clinicaltrials.gov/ct2/show/NCT02950064).[14] Although the NPDDS strategy has improved the efficacy of platinum-based drugs, data indicate that across nanoparticles tested, only a fraction (i.e., a median of 0.7%) of the injection dose is delivered to solid tumors,[15] therefore providing an opportunity for novel drug delivery systems to be developed and tested.

A more recent innovation is the use of nanoparticles based on plant viruses for the delivery of small-molecule drugs.[16–19] For example, tobacco mosaic virus (TMV) has been used to encapsulate *cis*-[Pt(NH_3)$_2$Cl(phenanthridine)](NO_3) (phenanthriplatin) via electrostatic interactions,[16] and cisplatin has been loaded into TMV particles by exploiting its coordination chemistry.[17] Both systems have been demonstrated to be effective in drug delivery and cancer cell killing in *in vitro* and *in vivo* some cases, whole plant viruses are used complete with the native genome, but viruslike particles (VLPs) comprising self-assembling coat proteins but no genome are easy to produce by expressing the monomeric structural proteins, yielding monodisperse and noninfectious protein cages suitable for further modification.[20] In previous work, we reported the assembly of VLPs based on Physalis mottle virus (PhMV) and systematically investigated their fate *in vitro* and *in vivo* by multimodal molecular imaging.[21,22] Among many advantages, the biocompatible and biodegradable PhMV particles achieved a long circulation halflife of ~44 h, the ability to target solid tumors *in vivo*, and efficient delivery with up to 6% of the injection dose remaining in the tumor.[21] These results paved the way for the development of PhMV-derived VLPs as a drug delivery platform.

Here, we designed a new NPDDS by conjugating maleimide-functionalized cisplatin (Pt-Mal) to the internal and/or external surface of PhMV-derived VLPs via a thiol—maleimide reaction. We prepared three sets of particles: one control set carrying the fluorescent label cyanine 5.5 (Cy5.5) for tracking and poly(ethylene glycol) (PEG) to improve biocompatibility (PhMVCy5.5-PEG), one as above but with the internal surface conjugated to cisplatin (Pt-PhMVCy5.5-PEG), and one with both the internal and external surfaces conjugated to cisplatin (Pt-PhMVCy5.5-Pt). We determined the physicochemical properties of the particles, evaluated the cisplatin release profiles, cell uptake, and cytotoxicity *in vitro*, and then tested the efficacy of the Pt-PhMVCy5.5-PEG particles *in vivo* using an MDA-MB-231 breast cancer murine xenograft model.

MATERIALS AND METHODS

Preparation of VLPs.

The Pt-Mal complex was synthesized by a modified literature procedure and fully characterized (Supporting Information, Figures S1–S6). VLPs were prepared by expressing PhMV coat protein subunits in *Escherichia. coli* as reported.[20] Pt-Mal was conjugated to cysteine residues on the internal surface of the PhMV particles by mixing 3 molar equiv per coat protein (eq/CP) of Pt-Mal with 2 mg/mL PhMV particles in 50 mM potassium phosphate buffer (pH 7.0, referred to as KP buffer) at room temperature overnight. The Pt-PhMV particles were then purified by 30% sucrose cushion ultracentrifugation (116,525 g, 1 h, room temperature). The Pt-PhMVCy5.5-PEG particles were prepared by resuspending the Pt-PhMV pellet in 50 mM phosphate buffer (pH 7.4), adding 0.2 eq/CP of Cy5.5-NHS, incubating for 3 h at room temperature, adding 5 eq/CP of 2000 Da mPEG-NHS (Nanocs, New York, NY, USA), and then incubating as above. The products were purified by ultracentrifugation as above followed by dialysis against 50 mM phosphate buffer (pH 7.4) overnight. The Pt-PhMVCy5.5-Pt particles were prepared by converting amine groups on the surface to thiols by reaction with 50 eq/CP of Traut's reagent (2-iminothiolane; Thermo

Fisher Scientific, Waltham, MA, USA) in 50 mM phosphate buffer (pH 7.4) for 3 h. The thiol-functionalized Pt-PhMV particles were purified by ultracentrifugation as above and dispersed in 50 mM phosphate buffer (pH 7.4) before adding 0.2 eq/CP of Cy5.5-NHS and incubating for 3 h at room temperature, then 3 eq/CP of Pt-Mal and incubating as above. The Pt-PhMVCy5.5-Pt products were purified by ultracentrifugation and dialysis as above. For the preparation of control PhMVCy5.5-PEG particles, Cy5.5 and PEG were added as described above but the reaction with Pt-Mal was omitted. All final products were dispersed and stored in 50 mM phosphate buffer (pH 7.4). The physical properties of the VLPs were characterized by UV/vis spectroscopy, native and denaturing gel electrophoresis, zeta potential, size exclusion chromatography (SEC), and transmission electron microscopy (TEM), as described in the Supporting Information.

Cisplatin Release Profile and Inductively Coupled Plasma Mass Spectrometry (ICP-MS).

The release of cisplatin from VLPs was investigated by dialyzing 200 μL of VLP suspension (3 mg/mL) against 12 mL of PBS (pH 7.4 or 6.4) or citrate buffer (pH 5.2) in Slide-A-Lyzer MINI dialysis tubes with a molecular weight cutoff of 10 kDa (Thermo Fisher Scientific) at 37 °C with gentle shaking. We collected 100 μL of the dialysis buffer every few hours over a period of 144 h for ICP-MS analysis of released platinum using a Thermo iCAP RQ instrument (Thermo Fisher Scientific).

Cytotoxicity toward Cancer Cell Lines.

The biocompatibility and cytotoxicity of the VLPs were determined using the 3-(4,5-dimethylthiazol-2-yl)-2,5-diphenyltetrazolium bromide (MTT) assay (ATCC, Manassas, VA, USA) and a panel of four human cancer cell lines: MDA-MB-231 (breast cancer), SKOV-3 (cisplatin-resistant ovarian cancer), A2780 (cisplatin-sensitive ovarian cancer), and PC-3 (prostate cancer). Cells were treated with each formulation normalized to cisplatin concentrations in the range of 0.01–50 μM in triplicate for 48 h and MTT assays were carried out according to the manufacturer's recommendations. Viability was determined by measuring the absorbance at 570 nm using an Infinite M200 plate reader (Tecan, Männedorf/Zürich, Switzerland). Each assay was performed in triplicate and the normalized cell proliferation values were averaged for each treatment concentration, allowing use for calculating IC_{50} values.

Analysis of Particle Uptake and Intracellular Distribution.

MDA-MB-231 cells were incubated with free Pt-Mal and Pt-PhMVCy5.5-PEG for 24 h and the uptake and intracellular distribution of platinum were determined by inductively coupled plasma mass spectrometry (ICP-MS), as indicated above. The cell components were separated using an NE-PER nuclear and cytoplasmic extraction kit (Thermo Fisher Scientific).

Fluorescence-Activated Cell Sorting (FACS).

Cells were grown to confluency, collected in enzyme-free Hank's-based cell dissociation buffer, and distributed in 200 μL aliquots at a concentration of 2×10^5 cell/mL in V-bottom 96-well plates. The VLPs were added to the cells at a final concentration of ~10 μg/mL

normalized to native PhMV particles (equivalent to 2×10^6 PhMV particles per cell) and incubated for 3 h. The cells were washed twice in FACS buffer (0.1 mL 0.5 M EDTA, 0.5 mL FBS, 1.25 mL 1 M HEPES, pH 7.0 in 50 mL PBS without Ca^{2+} and Mg^{2+}) and fixed in 2% (v/v) formaldehyde in FACS buffer for 10 min at room temperature. The cells were then washed and resuspended in FACS buffer and analyzed using an Accuri C6 flow cytometer (BD, Franklin Lakes, NJ, USA). Triplicates of each sample were maintained and at least 10,000 events (gated for live cells) were recorded. Data were analyzed using FlowJo v10.

In Vivo Chemotherapy and Biodistribution.

Animal experiments were carried out according to IACUC-approved procedures at the University of California San Diego. MDA-MB-231 cells were resuspended to a concentration of 1×10^6 cells per mL in a 1:1 ratio of RPMI medium and Matrigel (Corning Life Sciences, New York, NY, USA). We injected 100 μL of the cell suspension subcutaneously into the right hind leg of NCr nude mice (Charles River, Wilmington, MA, USA) at 4–6 weeks of age. The mice were treated with drugs or VLPs when the tumor volume reached ~150 mm^3 (~11 days postinjection). Treatment was administered intravenously twice weekly at a dosage of 1.0 mg/kg body weight normalized to Pt. Five independent groups of $n = 10$ animals were established (PBS, PhMVCy5.5-PEG, cisplatin, Pt-Mal, and Pt-PhMVCy5.5-PEG). Tumor size and body weight were measured before each injection and the volume was calculated using the formula $v = l \times w^2/2$. Mice were euthanized if the tumor size exceeded 1000 mm^3 according to IACUC guidelines. For biodistribution, mice ($n = 3$) were euthanized after three intravenous doses of cisplatin, Pt-Mal, or Pt-PhMVCy5.5-PEG in 24 h. Organs were collected and the Pt content was determined by ICP-MS, as described above.

RESULTS AND DISCUSSION

Synthesis and Characterization of PhMV Nanoparticles Loaded with Cisplatin-Maleimide.

PhMV nanoparticles were prepared by expressing the PhMV coat protein in *E. coli* as previously described,[20] resulting in the assembly of VLPs comprising 180 coat protein units. The internal and external surfaces present distinct chemical groups that can be functionalized independently: four lysine residues (K62, K143, K153, and K166) are exposed on the external surface of each subunit resulting in 720 addressable amine groups per particle, whereas a single cysteine residue (C75) is exposed on the internal surface resulting in 180 addressable thiol groups per particle.[21,23] The maleimide-functionalized Pt(IV) prodrug (Pt-Mal) features two additional axial maleimide groups allowing conjugation to cysteine residues via a thiol–maleimide Michael addition (Scheme 1).

Three types of nanoparticles were produced. The first was labeled with the fluorescent dye Cy5.5 to allow tracking in cells and *in vivo*, coated with PEG to prevent nonspecific uptake, and internally loaded with cisplatin(lV) derivative by conjugation to the exposed cysteine residues. This formulation was achieved by first conjugating Pt-Mal to the internal cysteine residues (Scheme 1A) and then reacting the Pt-PhMV nanoparticles with cyanine5.5 *N*-hydroxysuccinimide ester (Cy5.5-NHS) and succinimidyl poly(ethylene glycol) *N*-hydroxysuccinimide ester (mPEG-NHS) to modify the external surface (Scheme 1B). The

resulting particles were named Pt-PhMVCy5.5-PEG. Second, control particles were prepared by modifying the external surface with Cy5.5 and PEG as above but without the internal loading of the cisplatin(IV) derivative. The resulting particles were named PhMVCy5.5-PEG. Finally, the presence of 720 external lysine residues provided an opportunity to increase the cisplatin payload. The third set of particles was therefore prepared by converting some of the external amine groups to thiols using Traut's reagent, allowing subsequent reactions with Cy5.5-NHS to conjugate Cy5.5 to the remaining amines and with Pt-Mal to cover the internal and external surfaces with cisplatin (Scheme 1B). The resulting particles were named Pt-PhMVCy5.5-Pt. The latter particles were not conjugated with PEG because the addition of mPEG-SH reduced the Pt content of the particles. This result is consistent with recent reports showing that a retro-Michael reaction occurs when thiosuccinimide linkages encounter a competing thiol exchange reactant.[24,25]

All three VLP formats were purified by ultracentrifugation followed by dialysis against PBS (pH 7.4). The Pt and protein contents of the particles were measured by ICP-MS and the bicinchoninic acid (BCA) assay, respectively. The Pt-PhMVCy5.5-PEG and Pt-PhMVCy5.5-Pt particles contained 7.9 and 38.0 μg Pt per mg of protein, respectively, equivalent to ~155 and ~749 Pt molecules per particle. Given the availability of 180 Cys side chains on the internal surface and 720 Lys side chains on the exterior surface, high drug loading was achieved with 85% coverage achieved for Pt-PhMVCy5.5-PEG (180 available reaction sites) and 83% coverage achieved for Pt-PhMVCy5.5-Pt (180 + 720 total available reaction sites).

The morphology of the three modified VLPs was compared to native particles by TEM, as shown in Figure 1A. In all cases, the particles adopted the typical monodisperse and sphere-like icosahedral structure with a particle diameter of ~30 nm. During SEC, the particles eluted from a Superose6 column in a single peak at ~7.6 mL, indicating that the VLPs remained stable and dispersed in aqueous solution. Successful surface modification was confirmed by denaturing sodium dodecyl sulfate polyacrylamide gel electrophoresis (SDS-PAGE) followed by staining with Coomassie Brilliant Blue (Figure 1B) and by agarose gel electrophoresis (Figure 1C). SDS-PAGE analysis revealed a single 26 kDa band corresponding to the native PhMV coat protein. Following conjugation with Pt-Mal (M_r = 636 Da), Cy5.5 (M_r = 767 Da), and mPEG (M_r = ~2 k Da), an additional band of ~29 kDa was observed in the lanes containing PhMVCy5.5-PEG and Pt-PhMVCy5.5-PEG, reflecting the anticipated increase in mass of the coat protein and showing that the particles were mixtures of modified and unmodified subunits. For the Pt-PhMVCy5.5-Pt formulation, the smeared band at ~28 kDa indicates a mixture of coat proteins with both internal and external modification with cisplatin and/or Cy5.5 dyes. Fluorescent protein bands were present in all samples except the native VLP confirming successful covalent attachment of the fluorophore. Further densitometric analysis of the stained gel bands indicated ~41% coverage with PEG (~295 PEG chains per particle). The number of Cy5.5 molecules per particle was ~26, as determined by UV/visible spectroscopy and calculated using the Beer–Lambert law and Cy5.5 extinction coefficients. The changes in surface charge after modification were analyzed by zeta potential and agarose gel electrophoresis (Figure 1C) revealing that PEGylation of the external surface neutralized the positive amine groups, reducing the positive charge of PhMVCy5.5-PEG (+1.45 ± 0.51 mV) compared to the native

VLP (+4.42 ± 0.43 mV). However, the conjugation of Pt-Mal significantly changed the surface charge distribution of the VLP that brought the overall charge of the Pt-PhMVCy5.5-PEG particles close to neutral (+1.06 ± 0.45 mV). Further, the conjugation of Pt to the internal and external surfaces yielded a nanoparticle formulation with an overall negative surface charge of −7.52 ± 0.50 mV; the latter is also seen in the agarose gel electrophoresis with Pt-PhMVCy5.5-Pt migrating toward the anode. The differences in surface charge comparing Pt-PhMVCy5.5-PEG and Pt-PhMVCy5.5-Pt may be explained by the fact that a larger amount of Pt is reacted compared to PEG, and thus, more Lys side chains are neutralized.

Drug Release and Cytotoxicity *In Vitro*.

The dysregulation of pH is an adaptive feature of most cancers.[27] The intracellular pH (pH_i) of normal cells is ~7.2, which is slightly more acidic than the extracellular pH (pH_e) of ~7.4. In contrast, the extracellular environment of tumors *in vivo* (pH_e 6.2–6.9) is significantly more acidic than the intracellular pH (pH_i 7.12–7.65).[27] The low pH_e of the tumor environment facilitates the reduction of Pt(IV) maleimides to release cisplatin(II). We therefore evaluated the cisplatin release profile in a simulated acidic lysosomal compartment (citrate buffer, pH 5.2) and a simulated tumor microenvironment (PBS, pH 6.4) compared to the physiological pH of blood (PBS, pH 7.4). The low-pH environments significantly increased the Pt release rate (Figure 2A). We found that >60% of the Pt was released at pH 6.4 and >83% was released at pH 5.2 after 48 h, and a slow release rate was maintained over the rest of the 144 h time course. In contrast, <18% of the platinum was released at pH 7.4 and the release stopped after 72 h. The kinetics of the Pt release was fitted to the logarithmic increment, as shown in Figure S7. This result indicates that Pt-PhMVCy5.5-PEG can efficiently release its cargo in a model of the tumor microenvironment but retains its cargo in a model representing the physiological pH of the circulation, which is an ideal behavior for targeted delivery to tumors.

Next, we investigated the *in vitro* biocompatibility of the VLPs using the MTT assay in human breast cancer cell line MDA-MB-231 (Figure 2B). The viability of untreated cells was set as a control. Cells incubated with PhMVCy5.5-PEG at concentrations of 100–500 μg/mL remained >98% viable after 24 h and >91% viable after 48 h. The low *in vitro* cytotoxicity of the VLPs supports their use as an *in vivo* drug delivery vehicle. The efficacy of the cisplatin-loaded VLPs was investigated using a panel of cancer cells and was compared to free cisplatin and Pt-Mal using the MTT assay. The 50% inhibitory concentration (IC_{50}) was calculated for each formulation (normed to the Pt concentration) and is shown in Figure 2C, with detailed fitting profiles provided in Figure S8. The IC_{50} of cisplatin was adapted from the Genomics of Drug Sensitivity in Cancer database.[26] We found that cisplatin, Pt-Mal, and Pt-PhMVCy5.5-PEG showed equivalent toxicity toward the MDA-MB-231 and A2780 cancer cell lines and significantly improved the efficacy against the cisplatin-resistant ovarian cancer cell line SKOV-3 and PC-3 prostate cancer cells. There were no significant differences comparing the free Pt-Mal and Pt-PhMVCy5.5-PEG nanoparticle formulations, demonstrating that the prodrug retains its efficacy when delivered by the VLP. Contrary to our expectations, the Pt-PhMVCy5.5-Pt particles showed almost universally lower efficacy compared to the other three formulations despite the higher Pt

content, probably reflecting the strong negative surface charge of the particles, which caused repulsion at the negatively charged cell surface and thus inhibited particle uptake (see Figure 1C).

The uptake and intracellular distribution of the nanoparticle formulations were evaluated by laser confocal scanning microscopy (LCSM) (Figure S9) and flow cytometry (Figure 3A,B). MDA-MB-231 cells were incubated for 3 h with 10 μg/mL of each formulation (normalized to the mass of the capsid protein). We found that Pt-PhMVCy5.5-PEG particles were taken up more efficiently than either the PhMVCy5.5-PEG or Pt-PhMVCy5.5-Pt particles. Slightly positive or near neutral particles can be taken up more efficiently by cancer cells, and the higher intracellular drug concentration helps to overcome drug resistance while avoiding charge-induced toxicity *in vivo*.[3,28] These results supported the observed difference in cytotoxicity between Pt-PhMVCy5.5 and Pt-PhMVCy5.5-Pt (Figure 2C). The remarkable anticancer activity of cisplatin reflects its ability to bind the N7 atom of guanine bases, leading to DNA damage and cell death.[29] Therefore, we assessed the intracellular distribution of Pt in MDA-MB-231 cells following incubation with free Pt-Mal or Pt-PhMVCy5.5-PEG for 24 h. The cell components were separated using the NE-PER nuclear and cytoplasmic extraction kit and the Pt content of each component was determined by ICP-MS. We found that the total intracellular Pt content of cells incubated with Pt-PhMVCy5.5-PEG was 1.77-fold higher than in cells incubated with free Pt-Mal, and the differential was 1.76-fold for the cytosolic extract and 1.84-fold for the nuclear extract (Figure 3C,D). These results are consistent with the confocal and flow cytometry data, and similar uptake behavior was also observed in the prostate cancer cell line PC-3 (Figure S10).

Biodistribution and Cytotoxicity *In Vivo*.

Based on the *in vitro* cytotoxicity of Pt-PhMVCy5.5-PEG, we investigated the efficacy of this formulation *in vivo* using the xenograft tumor model of triple negative breast cancer (MDA-MB-231) in NCr nude mice. When the tumor volume reached ~150 mm^3, the mice were assigned to five groups as follows (n = 10 per group): (1) PBS as a negative control, (2) PhMVCy5.5-PEG (PhMV) as a nanoparticle control, (3) free cisplatin, (4) free Pt-Mal, and (5) Pt-PhMVCy5.5-PEG (Pt-PhMV). In groups 3–5, the dose was normalized to the Pt content, with each mouse receiving an intravenous bolus with a dose equivalent to 1.0 mg Pt per kg body weight administered twice weekly. The quantity of particles administered in group 2 was adjusted to match group 5. The disease burden and side effects were monitored twice weekly by examining the physical condition, body weight, and behavior of the animals according to the IACUC protocol.

Tumor growth was only slightly inhibited in the mice treated with cisplatin or Pt-Mal compared to the PBS control, but there was significant inhibition of tumor growth in the group treated with Pt-PhMV particles. We also noticed that the PhMV particle control group showed a slight delay in tumor growth (Figure 4A–C). This may reflect the ability of VLPs based on PhMV to stimulate an antitumor response by recruiting and activating innate immune cells in the tumor microenvironment.[30] Therefore, the greater efficacy Pt-PhMV could reflect a combination of drug delivery to tumor cells and innate immune response, and this synergistic activity will be investigated in more detail in future studies.

Our tumor growth data were supported by survivor curve analysis (Figure 4D). All mice in the PBS control group had succumbed to the disease by day 28, but >90% of the mice in group 5 (Pt-PhMV) remained alive at this stage, and survival was prolonged to 38 days. In comparison, the survival of the mice treated with free cisplatin was only prolonged to 31 days.

The biodistribution of the Pt in different organs was evaluated after three injections. Three mice from each group were randomly selected for euthanasia and the Pt content of each organ was measured by ICP-MS. Data indicate that the Pt-PhMV particles were successfully delivered to the tumor with 10-fold higher levels of Pt than the animals treated with Pt-Mal and 4.6-fold higher levels than the animals treated with cisplatin (Figure 5A). This result can be attributed to passive targeting based on the EPR effect of nanoparticles, consistent with our previous study.[21] The spleen and liver also took up substantially more Pt-PhMVCy5.5-PEG than Pt-Mal or cisplatin, which is consistent with the nanoparticle clearance pathway.[21] Over the course of the *in vivo* study, the mice treated with Pt-PhMVCy5.5-PEG showed no evidence of weight loss or abnormal behavior; the body weight increased slightly over the time course of treatment albeit at slightly slower rate compared to the other treatment arms or PBS controls (Figure 5B). The free drug also showed no off-target effects at the low dose we used. Taken together, these *in vivo* data confirm that Pt-PhMVCy5.5-PEG VLPs provide the basis for a safe and efficacious smart drug delivery system suitable for the treatment of solid tumors.

CONCLUSIONS

We have designed and synthesized cisplatin-loaded VLPs as a delivery system that allows the direct targeting of cancer cells for efficacious prodrug therapy. The systematic *in vitro* characterization of the Pt-PhMVCy5.5-PEG formulation confirmed the controlled release of cisplatin in a model of the tumor microenvironment and cytotoxicity toward a panel of cancer cells (including cisplatin-resistant cell lines). We then tested the VLPs *in vivo* and successfully inhibited the growth of tumors in a murine xenograft model, significantly increasing the survival of mice compared to those treated with free cisplatin. Our drug delivery system therefore addresses the clinical limitations of free cisplatin and offers a promising new approach to cancer therapy.

Supplementary Material

Refer to Web version on PubMed Central for supplementary material.

ACKNOWLEDGMENTS

This work was funded in part by grants from the National Institutes of Health R01-CA202814 and R01CA224605 to NFS. We thank Professor Stephen Lippard for valuable comments on this research and the final manuscript and Dr. Fang Wang of the Lippard lab for preparing and characterizing the Pt-maleimide derivative. We thank Dr. Hema Masarapu, Sri Venkateswara University, Tirupati, India for providing the plasmids for VLP expression.

REFERENCES

(1). Cancer Facts & Figures. https://www.cancer.org/content/dam/cancer-org/research/cancer-facts-and-statistics/annual-cancer-facts-and-figures/2019/cancer-facts-and-figures-2019.pdf (03/26/2020),

(2). Pushpakom S; Iorio F; Eyers PA; Escott KJ; Hopper S; Wells A; Doig A; Guilliams T; Latimer J; McNamee C; Norris A; Sanseau P; Cavalla D; Pirmohamed M Drug repurposing: progress, challenges and recommendations. Nat. Rev. Drug Discovery 2018, 18, 41–58. [PubMed: 30310233]

(3). Ghosh S Cisplatin: The first metal based anticancer drug. Bioorg. Chem 2019, 88, 102925. [PubMed: 31003078]

(4). Wang D; Lippard SJ Cellular processing of platinum anticancer drugs. Nat Rev Drug Discovery 2005, 4, 307–320. [PubMed: 15789122]

(5). Galluzzi L; Senovilla L; Vitale I; Michels J; Martins I; Kepp O; Castedo M; Kroemer G Molecular mechanisms of cisplatin resistance. Oncogene 2012, 31, 1869–1883. [PubMed: 21892204]

(6). Hossen S; Hossain MK; Basher MK; Mia MNH; Rahman MT; Uddin MJ Smart nanocarrier-based drug delivery systems for cancer therapy and toxicity studies: A review. J. Adv. Res 2019, 15, 1–18. [PubMed: 30581608]

(7). Wang B; Wang S; Zhang Q; Deng Y; Li X; Peng L; Zuo X; Piao M; Kuang X; Sheng S; Yu Y Recent advances in polymer-based drug delivery systems for local anesthetics. Acta Biomater. 2019, 96, 55–67. [PubMed: 31152941]

(8). Naguib YW; Rodriguez BL; Li X; Hursting SD; Williams RO III; Cui Z Solid Lipid Nanoparticle Formulations of Docetaxel Prepared with High Melting Point Triglycerides: *In Vitro* and *in Vivo* Evaluation. Mol. Pharmaceutics 2014, 11, 1239–1249.

(9). Mukerabigwi JF; Ge Z; Kataoka K Therapeutic Nanoreactors as In Vivo Nanoplatforms for Cancer Therapy. Chem. - Eur. J 2018, 24, 15706–15724. [PubMed: 29572992]

(10). Cao J; Li X; Tian H Metal-Organic Framework (MOF)-Based Drug Delivery. Curr. Med. Chem 2019, 27, 1–5969.

(11). He Q; Shi J MSN Anti-Cancer Nanomedicines: Chemotherapy Enhancement, Overcoming of Drug Resistance, and Metastasis Inhibition. Adv. Mater 2014, 26, 391–411. [PubMed: 24142549]

(12). Peer D; Karp JM; Hong S; Farokhzad OC; Margalit R; Langer R Nanocarriers as an emerging platform for cancer therapy. Nat. Nanotechnol 2007, 2, 751–760. [PubMed: 18654426]

(13). Torchilin VP Recent advances with liposomes as pharmaceutical carriers. Nat. Rev. Drug Discovery 2005, 4, 145–160. [PubMed: 15688077]

(14). Zheng YR; Suntharalingam K; Johnstone TC; Yoo H; Lin W; Brooks JG; Lippard SJ Pt(IV) prodrugs designed to bind non-covalently to human serum albumin for drug delivery. J. Am. Chem. Soc 2014, 136, 8790–8798. [PubMed: 24902769]

(15). Wilhelm S; Tavares AJ; Dai Q; Ohta S; Audet J; Dvorak HF; Chan WCW. Analysis of Nanoparticle Delivery to Tumours. Nat. Rev. Mater 2016, 1, 16014.

(16). Czapar AE; Zheng Y-R; Riddell IA; Shukla S; Awuah SG; Lippard SJ; Steinmetz NF Tobacco Mosaic Virus Delivery of Phenanthriplatin for Cancer therapy. ACS Nano 2016, 10, 4119–4126. [PubMed: 26982250]

(17). Franke CE; Czapar AE; Patel RB; Steinmetz NF Tobacco Mosaic Virus-Delivered Cisplatin Restores Efficacy in Platinum-Resistant Ovarian Cancer Cells. Mol. Pharmaceutics 2018, 15, 2922–2931.

(18). Finbloom JA; Han K; Aanei IL; Hartman EC; Finley DT; Dedeo MT; Fishman M; Downing KH; Francis MB Stable Disk Assemblies of a Tobacco Mosaic Virus Mutant as Nanoscale Scaffolds for Applications in Drug Delivery. Bioconjugate Chem. 2016, 27, 2480–2485.

(19). Cao J; Guenther RH; Sit TL; Opperman CH; Lommel SA; Willoughby JA Loading and Release Mechanism of Red Clover Necrotic Mosaic Virus Derived Plant Viral Nanoparticles for Drug Delivery of Doxorubicin. Small 2014, 10, 5126–5136. [PubMed: 25098668]

(20). Ranjith-Kumar CT; Gopinath K; Jacob ANK; Srividhya V; Elango P; Savithri HS Genomic Sequence of Physalis Mottle Virus and Its Evolutionary Relationship with Other Tymoviruses. Arch. Virol 1998, 143, 1489–1500. [PubMed: 9739328]

(21). Hu H; Masarapu H; Gu Y; Zhang Y; Yu X; Steinmetz NF Physalis Mottle Virus-like Nanoparticles for Targeted Cancer Imaging. ACS Appl. Mater. Interfaces 2019, 11, 18213–18223. [PubMed: 31074602]

(22). Masarapu H; Patel BK; Chariou PL; Hu H; Gulati NM; Carpenter BL; Ghiladi RA; Shukla S; Steinmetz NF Physalis Mottle Virus-Like Particles as Nanocarriers for Imaging Reagents and Drugs. Biomacromolecules 2017, 18, 4141–4153. [PubMed: 29144726]

(23). Sri Krishna S; Sastri M; Savithri HS; Murthy MRN Structural Studies on the Empty Capsids of Physalis Mottle Virus. J. Mol. Biol 2001, 307, 1035–1047. [PubMed: 11286554]

(24). Ravasco JMJM; Faustino H; Trindade A; Gois PMP Bioconjugation with Maleimides: A Useful Tool for Chemical Biology. Chem. - Eur. J 2019, 25, 43–59. [PubMed: 30095185]

(25). Lyon RP; Setter JR; Bovee TD; Doronina SO; Hunter JH; Anderson ME; Balasubramanian CL; Duniho SM; Leiske CI; Li F; Senter PD Self-hydrolyzing maleimides improve the stability and pharmacological properties of antibody-drug conjugates. Nat. Biotechnol 2014, 32, 1059–1062. [PubMed: 25194818]

(26). Genomics of Drug Sensitivity in Cancer. https://www.cancerrxgene.org/ (01/08/2019),

(27). Shirmanova MV; Druzhkova IN; Lukina MM; Matlashov ME; Belousov VV; Snopova LB; Prodanetz NN; Dudenkova VV; Lukyanov SA; Zagaynova EV Intracellular pH imaging in cancer cells *in vitro* and tumors *in vivo* using the new genetically encoded sensor SypHer2. BBA-Gen. Subjects 2015, 1850, 1905–1911.

(28). Wang S; Huang P; Chen X Hierarchical Targeting Strategy for Enhanced Tumor Tissue Accumulation/Retention and Cellular Internalization. Adv. Mater 2016, 28, 7340–7364. [PubMed: 27255214]

(29). Min Y; Mao C-Q; Chen S; Ma G; Wang J; Liu Y Combating the Drug Resistance of Cisplatin Using a Platinum Prodrug Based Delivery System. Angew.Chem. Int. Ed 2012, 51 , 6742–6747.

(30). Lizotte PH; Wen AM; Sheen MR; Fields J; Rojanasopondist P; Steinmetz NF; Fiering S *In situ* vaccination with cowpea mosaic virus nanoparticles suppresses metastatic cancer. Nat. Nanotechnol 2016, 11, 295–303. [PubMed: 26689376]

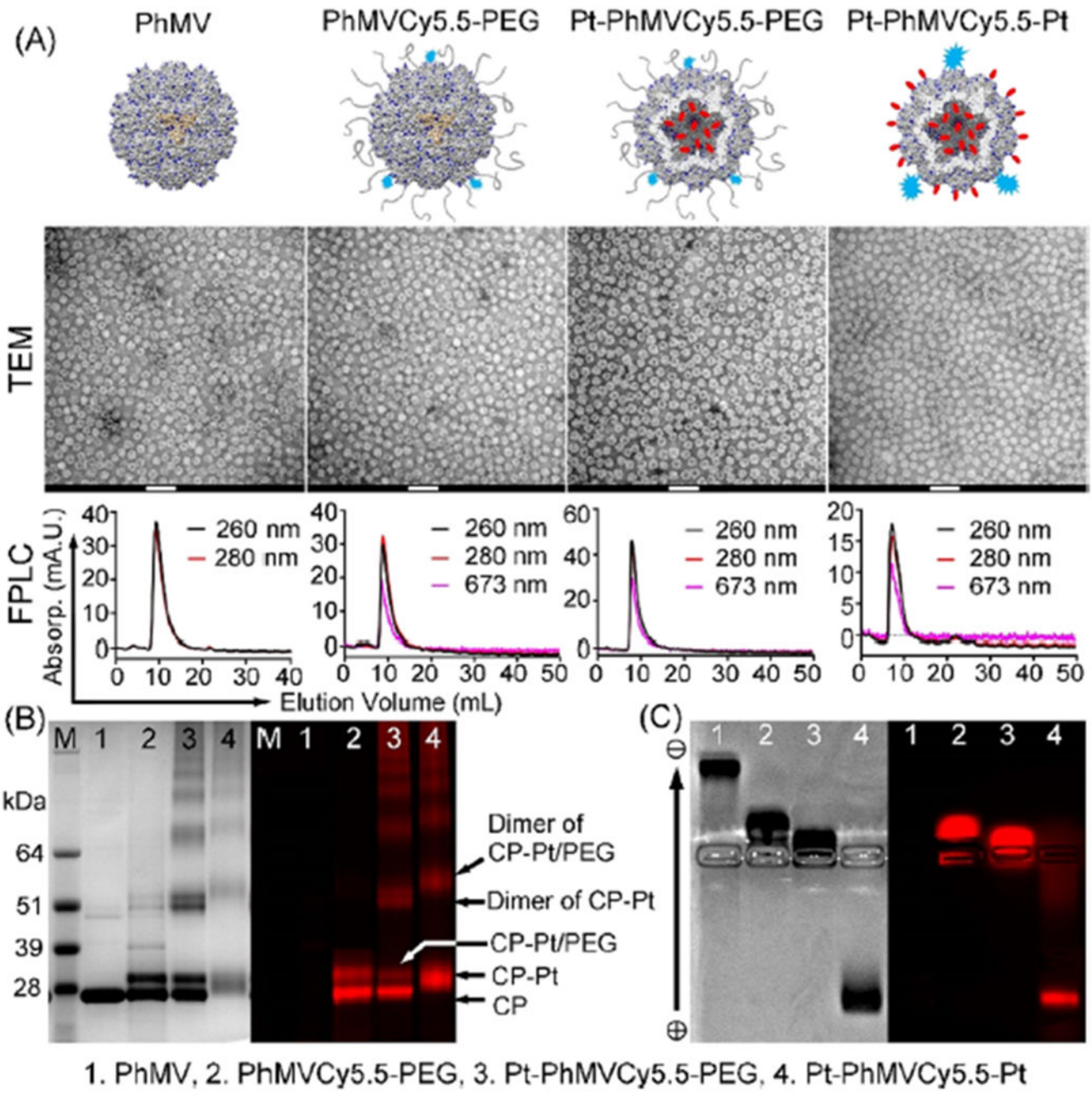

Figure 1.

Physicochemical characterization of PhMV-based nanoparticles. (A) Cartoon, TEM image (scale bars: 100 nm), and size exclusion chromatography profile of native PhMV and the three VLPs: PhMVCy5.5-PEG, Pt-PhMVCy5.5-PEG, and Pt-PhMVCy5.5-Pt. (B) SDS-PAGE analysis of the four nanoparticles followed by staining with Coomassie Brilliant Blue (left) or fluorescence imaging (right). (C) Agarose gel electrophoresis of the four nanoparticles followed by staining with Coomassie Brilliant Blue (left) or fluorescence imaging (right).

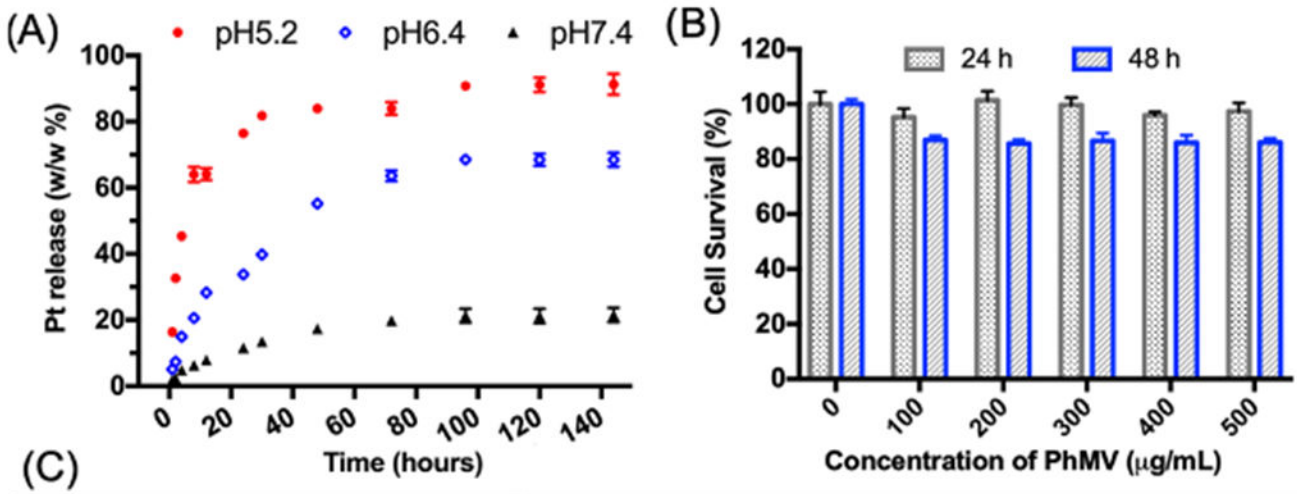

Cell line	Cancer type	IC50 in μM			
		Cis-Pt *	Pt-Mal	Pt-PhMV	Pt-PhMV-Pt
MDA-MB-231	Breast cancer	3.87	3.96±0.31	2.43±0.27	6.05±1.04
SKOV-3	Ovarian cancer	29.7	1.83±0.48	1.66±0.28	5.02±0.77
A2780	Ovarian cancer	0.88	0.87±0.15	0.84±0.14	9.75±0.58
PC-3	Prostate cancer	8.33	1.39±0.34	1.36±0.16	4.76±0.57

Figure 2.

Platinum release from nanoparticles and the comparative toxicity of nanoparticles and free drugs. Data from triplet experiments and standard deviations are shown. (A) Cisplatin release profiles from nanoparticles in pH-adjusted solutions. (B) Cytotoxicity of the control particle PhMVCy5.5-PEG determined by the MTT assay in MDA-MB-231 cells. (C) IC_{50} values (mean values ± standard deviations) of free cisplatin, Pt-Mal, Pt-PhMVCy5.5-PEG, and Pt-PhMVCy5.5-Pt particles against a panel of cancer cells determined by the MTT assay. All concentrations were normalized to Pt. Asterisk: ref.[26]

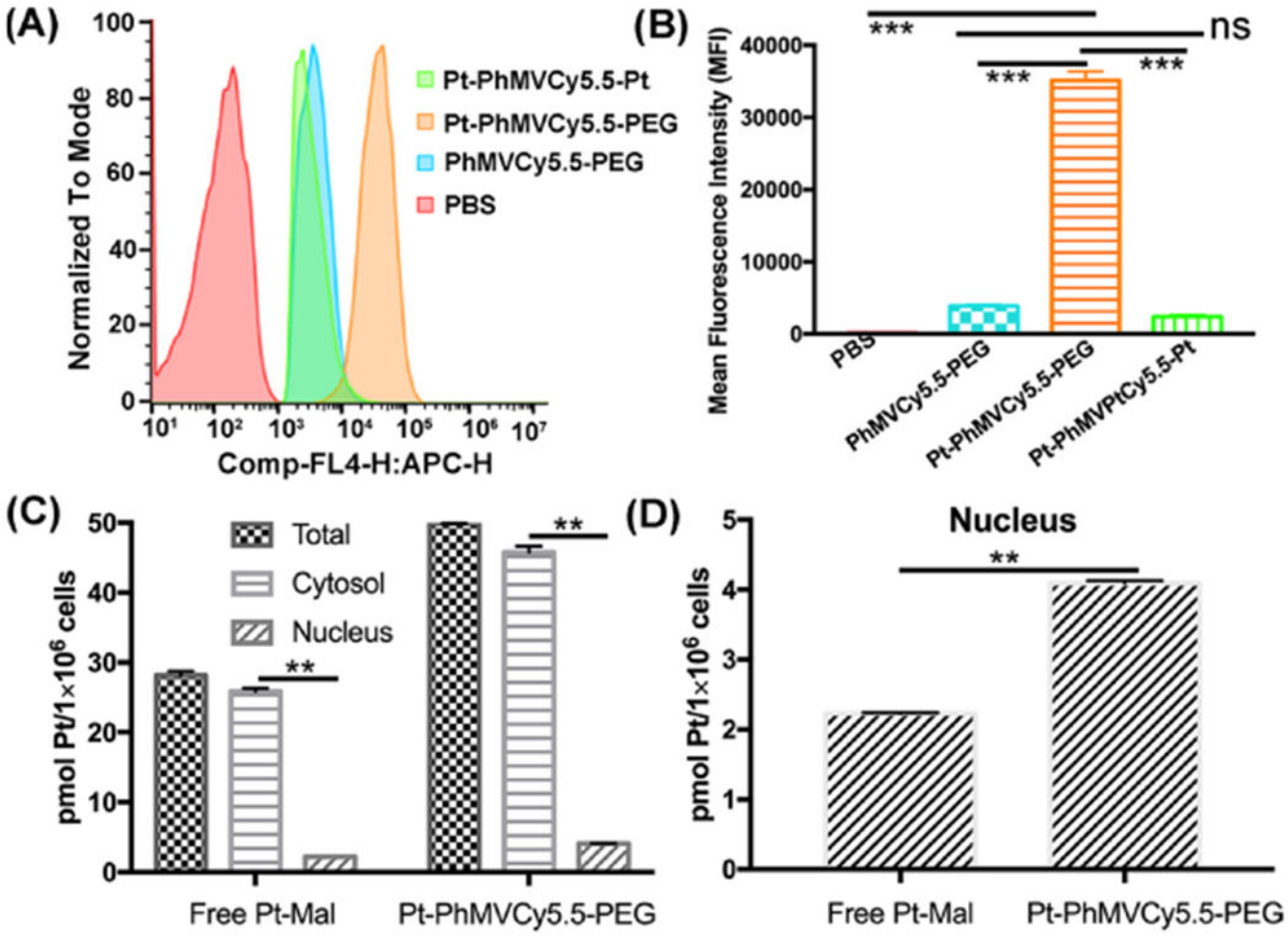

Figure 3.

Analysis of VLP uptake and distribution within MDA-MB-231 cells. (A) Quantitative analysis by flow cytometry and (B) mean fluorescence intensities (MFIs) of cells in each sample ($n = 3 \pm$ standard deviations, $^{***}p < 0.001$ per Student's t-test). Data were analyzed using FlowJo v10. (C, D) Intracellular distribution and nuclear content of Pt following the incubation of MDA-MB-231 cells with free Pt-Mal or Pt-PhMVCy5.5-PEG for 24 h ($^{**}p < 0.01$).

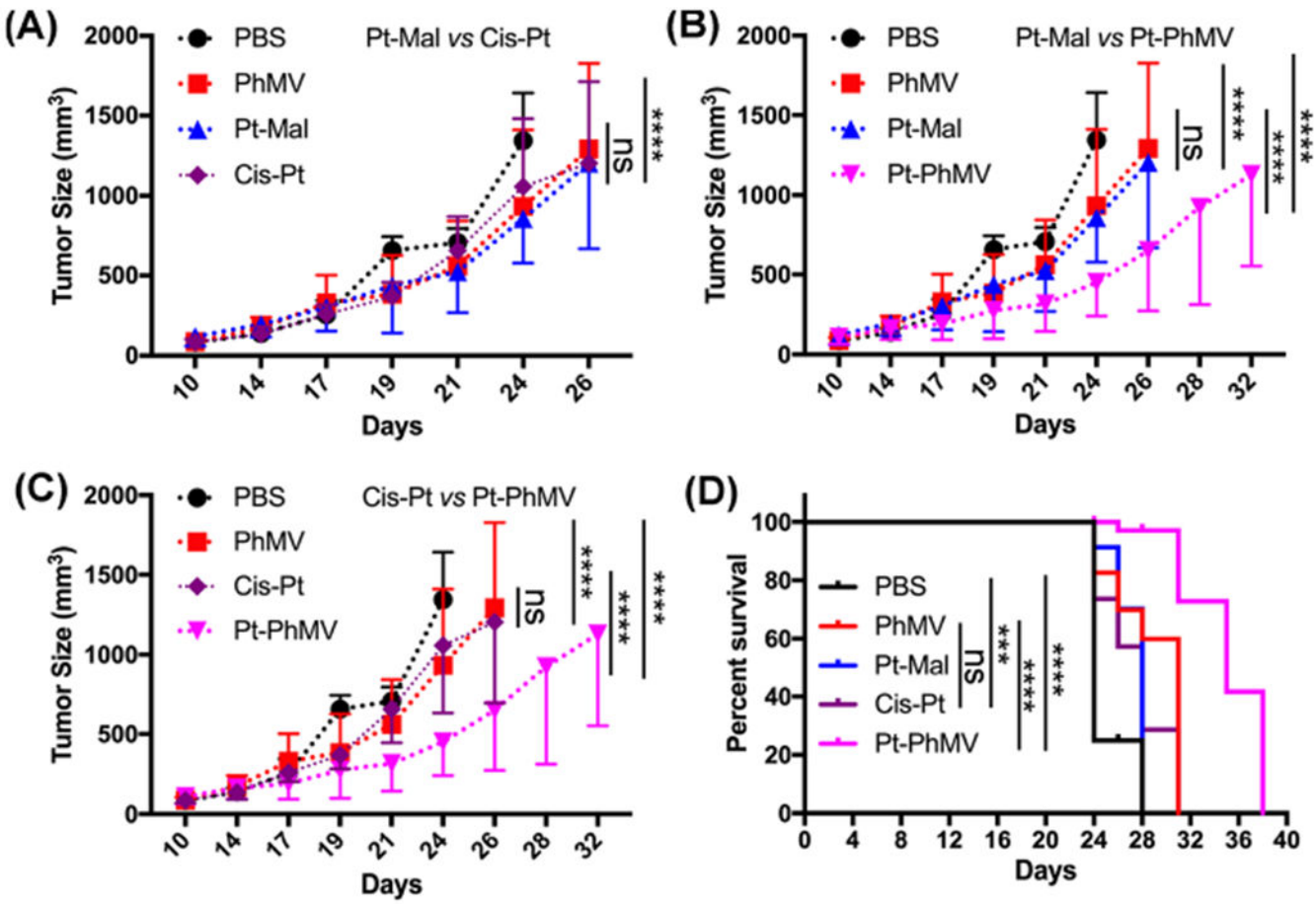

Figure 4.

Inhibition of tumor growth in an athymic mouse model ($n = 10$) with MDA-MB-231 xenografts after treatment with different formulations. The treatment began when tumors reached a volume of ~150 mm^3 and involved a twice-weekly intravenous bolus of 1.0 mg Pt/kg in the form of cisplatin (cis-Pt), Pt-Mal, or Pt-PhMVCy5.5-PEG (Pt-PhMV). PBS or PhMVCy5.5-PEG (PhMV) particles were administered as controls, with PhMVCy5.5-PEG particle dosage normalized to Pt-PhMVCy5.5-PEG. Tumor volumes and body weight were measured before each injection. Statistical analysis was carried out by two-way ANOVA. Mean tumor volumes and standard errors of the mean are shown. (A) Pt-Mal vs cis-Pt, (B) Pt-Mal vs Pt-PhMV, and (C) cis-Pt vs Pt-PhMV. (D) Statistical analysis for survival curves: log-rank (Mantel–Cox) test. ns = no statistical significance, ***: $p < 0.001$, ****: $p < 0.0001$.

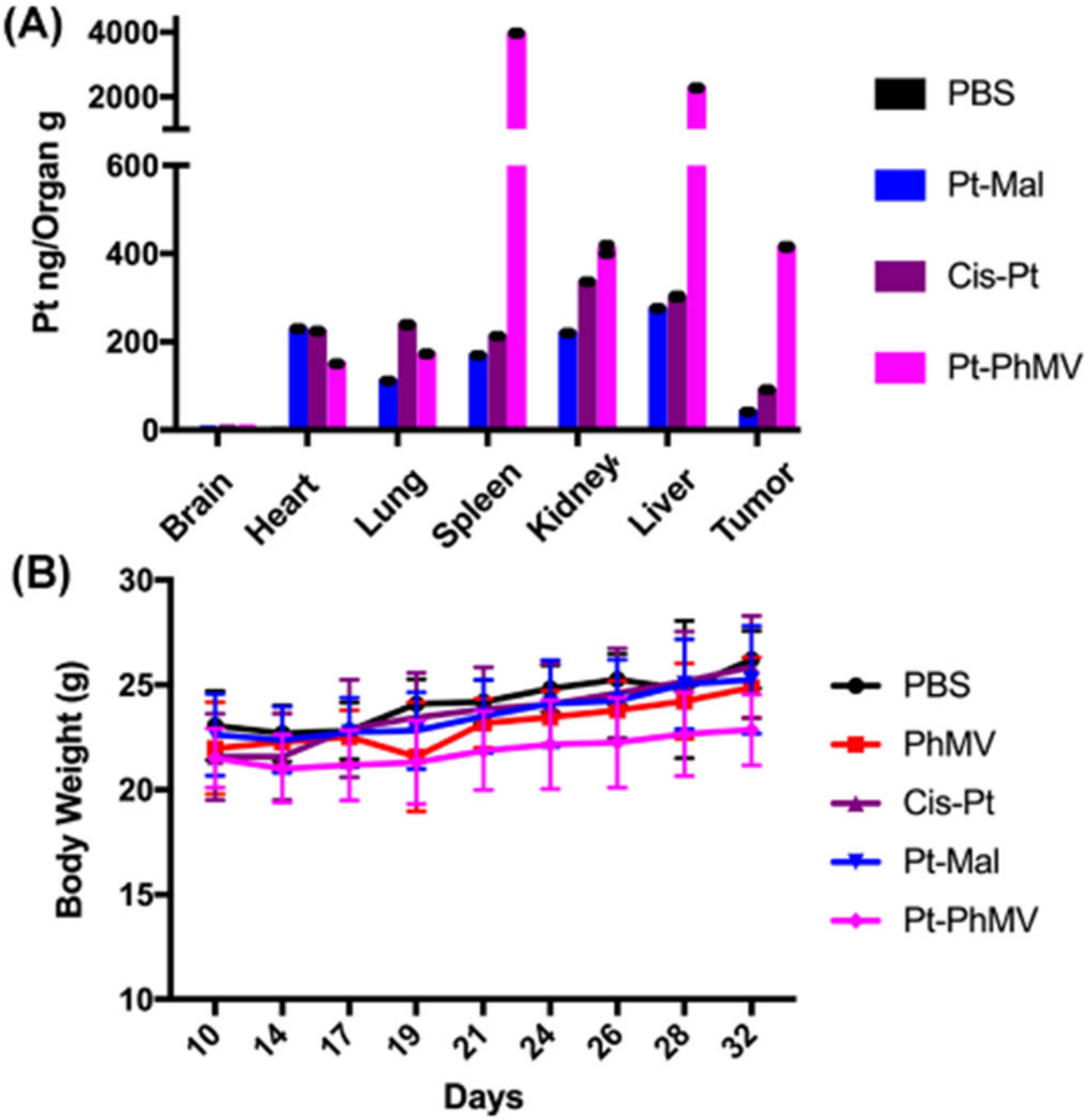

Figure 5.

(A) Biodistribution of Pt in organs/tissues as determined by ICP-MS after three injections of PBS, Pt-Mal, cisplatin (cis-Pt), or Pt-PhMVCy5.5-PEG (Pt-PhMV). (B) Body weight of tumor bearing mice over the course of the study. For (A) and (B), mean values ± standard deviations are shown.

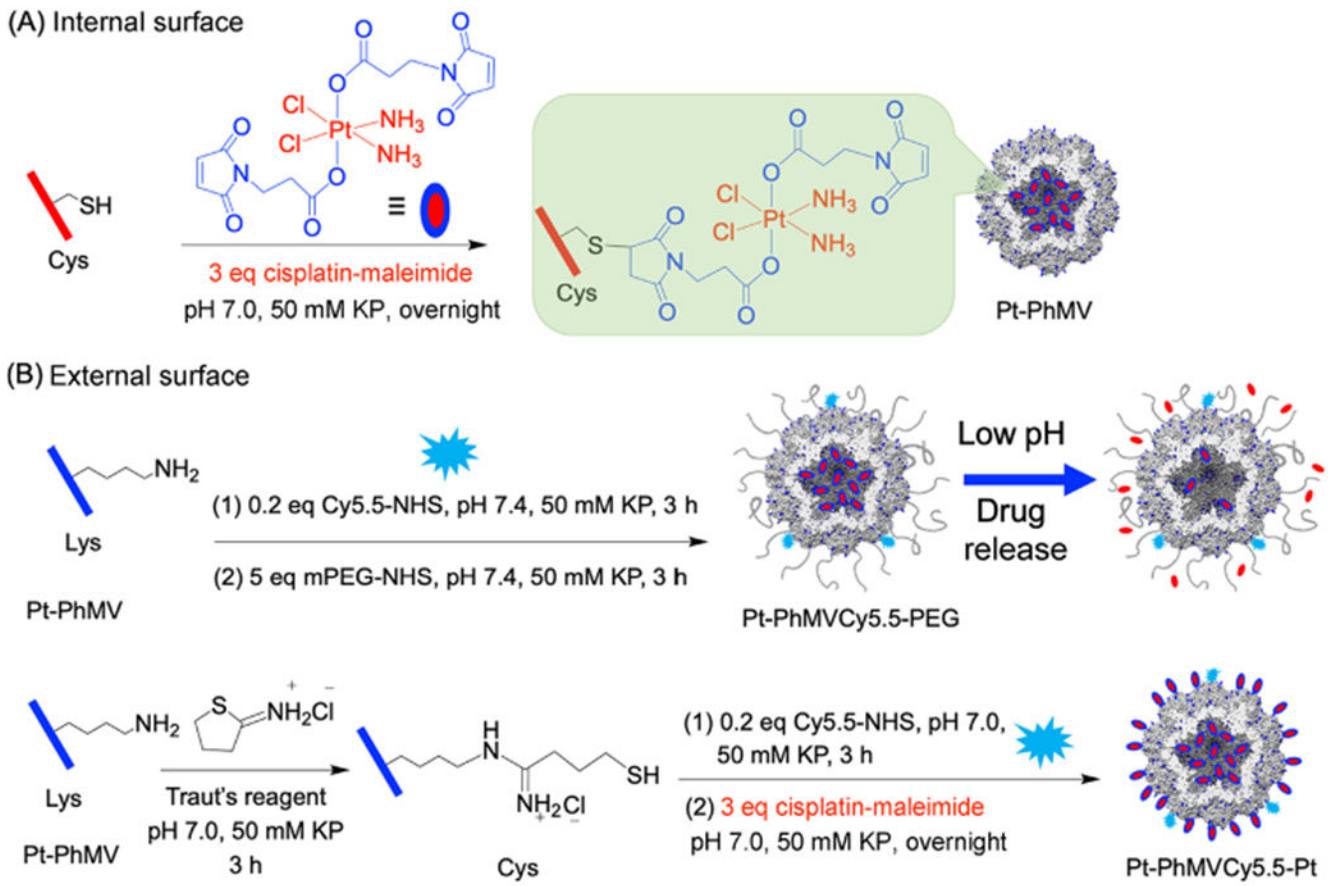

Scheme 1.

Strategies for the internal (A) and external (B) surface functionalization of VLPs based on PhMV